Main insights from 2D/3D poroelastic analysis of tunnel excavation in low permeability anisotropic ground

Lina-María Guayacán-Carrillo, Jean Sulem, Siavash Ghabezloo

Main insights from 2D/3D poroelastic analysis of tunnel excavation in low permeability anisotropic ground

Lina-María Guayacán-Carrillo*, Jean Sulem, Siavash Ghabezloo

Navier, Ecole des Ponts, Univ Gustave Eiffel, CNRS, Marne-la-Vallée, 77455 France

* Corresponding author

E-mail: lina.guayacan@enpc.fr

Abstract

Pore pressure evolution induced by tunnel excavation in low permeability anisotropic ground is investigated by means of a fully coupled hydro-mechanical finite element simulation. The goal is to explore the main trends of the pore pressure evolution on the basis of a poroelastic analysis, taking into account: on the one hand, the influence of excavation and face advance; on the other hand, the inherent anisotropy of the material. It is shown that overpressures can be induced before the passage of the face, depending on: the consolidation time of the rock, the rate of excavation and the degree of anisotropy of both the material and the initial stress state. Finally, a discussion about pore pressure evolution at tunnel wall is presented. An analysis is performed in order to propose a pore pressure release rate at the tunnel wall for 2D models.

Keywords

Poroelasticity, Hydro-mechanical coupling, Low-permeability ground, Tunneling excavation, Anisotropy, Overpressure

1. Introduction

Tunneling excavation performed in low permeability anisotropic ground has shown a significant influence of the excavation progress on pore pressure evolution. Indeed, continuous monitoring during excavations performed in claystone formations [1-5], showed induced overpressures before and after the passage of the tunnel face. Moreover, it has been observed that the amplitude of pore pressure change in the ground depends upon the distance to the face and to the tunnel wall.

Analysis of hydro-mechanical response to excavation progress is of major concern for tunnels design, mainly when it is excavated in low permeability ground. Indeed, understanding this response is a key issue for an adequate support design. As shown in recent analysis of excavation works in a claystone formation [5, 6], the response of the rock mass to the excavation progress exhibits a strong interplay between the pore pressure evolution and the induced fractured zone development around the tunnel. By analyzing the occurrence of tensile zones due to significant pore overpressure around the excavation, Guayacán-Carrillo et al. [6] have pointed out the key role of the hydro-mechanical coupling on the development of the failed zone around the tunnels. Thereafter, Vu et al. [5] have shown that a more realistic description of pore pressure change in the ground can be obtained by taking into account the shape and the extension of the excavation induced fractured zone. Nevertheless, the understanding of this interplay remains a challenging topic.

Among the recent studies on the pore-pressure evolution induced by excavation in claystone formations, one can mention: analysis of in-situ measurements [1, 2, 7-12]; numerical analysis based on models using transversely isotropic poroelastic behavior [6], anisotropic elastic and isotropic plastic behavior [13,14] and anisotropic elasto-visco-plastic behavior [15]; hydro-mechanical analysis and coupled modeling of the excavation damaged

zone based on strain localization analysis [16,17]. Even though the development of different numerical models has allowed significant progress in the simulation of the in-situ observations, further studies are still needed. Most of the existing works study the pore pressure evolution after the passage of the tunnel face using 2D simulations. However, for excavations in low permeability ground, pore pressure changes can also be observed before the passage of the tunnel face. Thus a careful evaluation of the overpressures observed before the passage of the tunnel face and the understanding of the physical mechanisms that control their evolution in time is of key importance for the assessment of the tunnel design.

In this paper, the pore pressure evolution induced by tunnels excavation is investigated using a 3D fully coupled hydro-mechanical finite element simulation, in the framework of a poroelastic analysis. The analysis is performed by taking into account different features that can influence the pore pressure evolution such as: the excavation rate, the permeability of the ground, the anisotropy of the material and of the initial stress state. Results obtained are analyzed and compared to in-situ measurements. As 2D models are more frequently used in tunnel design, a comparison between 3D and 2D numerical simulations is presented. A pore pressure release rate at the tunnel wall is proposed in an attempt to take into account the pore pressure evolution in a 2D model. This aims to propose a simplified numerical approach that accounts for the influence of the face advance and that can be directly used in engineering practice.

2. Theoretical framework

A fully coupled poroelastic analysis is performed using the finite element method to simulate the pore pressure evolution induced by tunnel excavation. The main goal of this analysis is to reproduce and understand the main trends of the pore pressure evolution with a simple

constitutive model taking into account the influence of the elastic anisotropy of the material and the advance of the tunnel face.

2.1. Poroelastic constitutive equations

The bases of poroelasticity theory have been presented in several textbooks and reference papers (e.g. [18, 19]). In this analysis, it is assumed that the porous material is fully saturated and under isothermal conditions.

Assuming negative compressive stress, the poroelastic constitutive equations are given by Eq. (1), where C_{ijkl} is the drained stiffness tensor, ε_{kl} the strain tensor, p the pore pressure and b_{ij} the Biot effective stress coefficient tensor [20, 21]. For an isotropic porous material, the Biot effective stress coefficient is given by $b = 1 - K_d/K_s$, where K_d is the drained bulk modulus and K_s is the unjacketed bulk modulus. The Lagrangian porosity variation is given by Eq. (2).

$$d\sigma_{ij} = C_{ijkl} d\varepsilon_{kl} - b_{ij} dp \qquad 1$$

$$d\phi = b_{ij} d\varepsilon_{ij} + \frac{1}{N} dp \qquad 2$$

where N is the Biot's skeleton modulus. For an isotropic material $1/N = b/K_s - \phi_0/K_\phi$, where K_ϕ is the unjacketed pore volume modulus [22, 23]. The coupling equation between the volumetric strain and the pore pressure change can be obtained by writing the fluid mass conservation $\mathrm{d}m_f = 0$ (where $m_f = \rho_f \phi$ is the fluid mass per unit volume) and by using Darcy's law for the fluid. Finally, the stress equilibrium and the fluid mass conservation give the system of coupled equations to solve:

$$\nabla \cdot \left(C_{ijkl} d\varepsilon_{kl} - b_{ij} dp \right) = 0 \qquad 3$$

$$b_{ij}\frac{d\varepsilon_{ij}}{dt}+\left(\frac{1}{N}+\frac{\phi_0}{K_f}\right)\frac{dp}{dt}-\frac{1}{\rho_f}\nabla\cdot\left(\rho_f\frac{k}{\mu}\nabla p\right)=0 \quad (4)$$

where ρ_f is the fluid specific mass, K_f is the fluid compression modulus, μ is the fluid viscosity and $\boldsymbol{k}$ is the intrinsic permeability tensor.

In undrained conditions, the mass of pore fluid remains constant. Therefore, the pore pressure change can be expressed as $\mathrm{d}p = -Mb_{ij}\mathrm{d}\varepsilon_{ij}$, where M is the Biot undrained modulus ($1/M = 1/N + \phi_0/K_f$).

2.2. Pore pressure diffusion and characteristic times during tunnel excavation

Pore pressure response obtained around tunnel excavation is related to two characteristics times. The first one, the consolidation characteristic time (t_c) of the host rock; the second one, the excavation time related to the pore pressure evolution (t_p). The consolidation characteristic time is evaluated by extending the solution of one-dimensional elastic consolidation to a problem of tunnel excavation by [24-26]:

$$t_c = \frac{L^2}{C_v} \quad (5)$$

with L a length characterizing the considered consolidation problem. In the literature this distance is set to tunnel radius ($L = D/2$) for deep tunnels [24, 27]. C_v is the consolidation coefficient defined as:

$$C_v = \frac{k}{\mu S} \quad (6)$$

where S is the storage coefficient given by [28]:

$$S = \frac{b}{K_d} + \phi_0 \left(\frac{1}{K_f} - \frac{1}{K_\phi}\right) \quad (7)$$

The excavation time t_p, which is related to the excavation rate and to the distance within which pore pressure changes are influenced by the tunnel face advance, is defined as [27]:

$$t_p = \frac{x_0 - x_f}{v} \quad (8)$$

where x_0 is the first location where pore pressure starts to deviate from its initial value; x_f the location where the response becomes independent of the tunnel face advance; v the tunnel excavation rate.

Therefore, the ratio t_c/t_p is given by:

$$\frac{t_c}{t_p} = \frac{v}{C_v} \frac{L^2}{(x_0 - x_f)} \quad (9)$$

3. Poro-elastic 3D finite element simulation of tunnel excavation

Tunnel excavation affects the surrounding rock ahead of the face. The deconfinement effect is active before the passage of the face and influences the pore pressure field. Therefore, the accurate simulation and interpretation of the overpressure observed before the passage of the face and its evolution in time must be achieve.

Hydro-mechanical modeling is performed using the finite element program ABAQUS/CAE. For the sake of completeness, the analysis has been performed taking into account different features that can influence the pore pressure evolution around tunnel

excavation. Hence, three different cases have been studied. In a first step, an isotropic axisymmetric model is considered in order to analyze the impact of the excavation rate and of the permeability of the ground (Case 1). Then, in a second step, simulations using a 3D model are performed to study the influence of the anisotropy of the material (Case 2) and of the initial stress state (Case 3). Finally, the obtained results are analyzed and compared to in-situ measurements.

3.1. Isotropic case – Axisymmetric model

Considering a radius of the tunnel R =2.6 m, the size of the finite element model is 80 m × 104 m. Fig. 1 shows the model geometry, the finite element mesh, and the initial and boundary conditions. Mesh validation of the model is presented in Appendix A. We consider 22 steps of excavation, corresponding to 52.8 m of excavation. A zero pore pressure is imposed at the tunnel wall, in order to simulate the excavation advance. The elastic parameters considered for this simulation are taken from Guayacán-Carrillo et al. [6] and are presented in Table 1. The unjacketed bulk modulus is K_s = 21.7 GPa, based on laboratory works performed by Belmokhtar et al. [29].

Table 1. Elastic mechanical and hydraulic parameters

Cases	$\sigma_{x,0}$ (MPa)	$\sigma_{y,0}$ (MPa)	E_x (MPa)	v	k (m/s)	ϕ_0
1	12.4		5200	0.3	variable	0.18

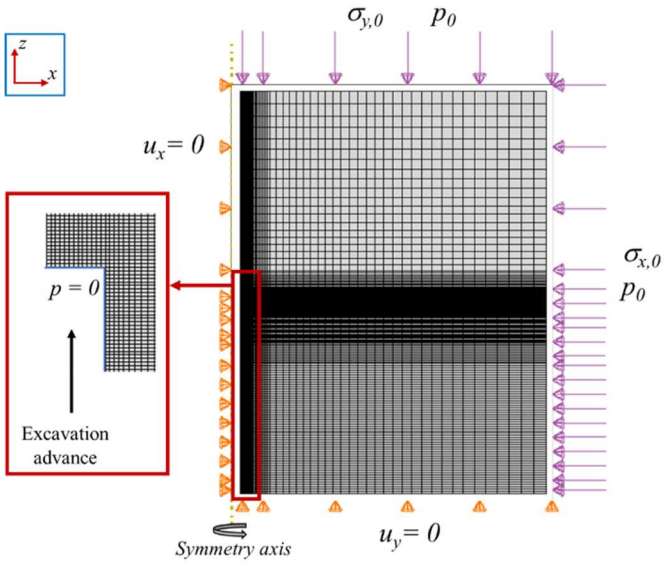

Fig. 1. Initial and boundary conditions for an axisymmetric model ($\sigma_{x,0}$ and $\sigma_{y,0}$ are the initial horizontal and vertical stresses and p_0 is the initial pore pressure).

A sensitivity analysis is performed by varying the ground permeability. Table 2 summarizes the set of parameters used in each studied case. The ratios t_c/t_p and v/k are also given. As explained by Anagnostou [30], for a given value of the storage coefficient of the ground, the ratio v/k governs the stability, the deformations and the ground pressure acting upon a shield or a lining in the vicinity of the face. It is observed that depending on the ratios t_c/t_p or v/k, the pore pressure evolution exhibits some differences, as explained below.

Table 2. Summary of different studied cases

Cases	1.a	1.b	1.c	1.d	1.e
v (m/week)	2.4	2.4	2.4	2.4	2.4
k (m/s)	2.7E-13	5.4E-13	2.7E-12	5.4E-12	2.7E-11
t_c/t_p	>1	>1	>1	≈1	<1
v/k	1.5E7	7.3E6	1.5E6	7.3E5	1.5E5

Pore pressure evolution induced by tunnel advance is studied before and after the passage of the tunnel face. Various distances from the tunnel wall and also from the tunnel face are considered for the analysis. In the following, the tunnel will be referred as z axis; the horizontal and vertical axes in a cross section will be referred as x axis and y axis, respectively. Fig. 2 shows the different positions analyzed in this section.

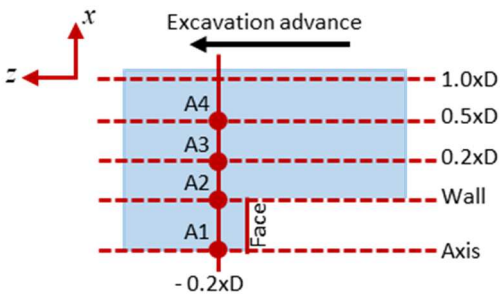

Fig. 2. Position of the studied sections. In dashed lines, sections followed at different distances on x axis (distances are given with respect to the tunnel wall). Points A1 to A4 are selected points located ahead of tunnel face, at a distance of $0.2 \times D$ (D is the tunnel diameter).

3.1.1. Pore pressure evolution observed as a function of the distance to the tunnel wall

Fig. 3 presents the pore pressure evolution of four different sections on the x axis: (a) In the axis of excavation, (b) at $0.2 \times D$ (D is the tunnel diameter) from the tunnel wall , (c) at $0.5 \times D$ from tunnel wall and (d) at $1.0 \times D$ from the tunnel wall. Pore pressure evolution is presented before and after the passage of the tunnel face, along the z axis.

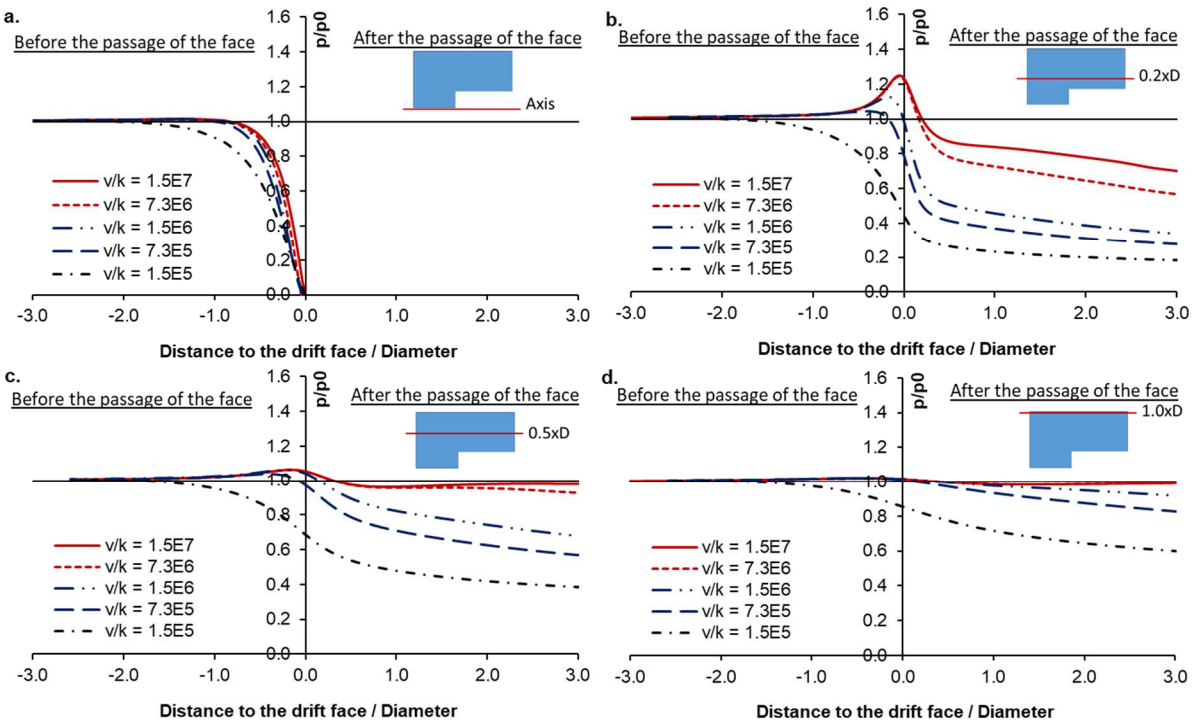

Fig. 3. Pore pressure evolution induced by tunnel excavation in an isotropic elastic medium with a ratio *v/k* = 1.5E5 to 1.5E7. Sections located on the *x* axis at: a. In the axis of excavation; b. At $0.2 \times D$ from the tunnel wall; c. At one radius ($0.5 \times D$) from the tunnel wall; d. At one diameter (D) from the tunnel wall.

For the case 1.e, with a lower *v/k* ratio (1.5E5), the pore pressure evolution depends on the distance to the tunnel wall (i.e. in the direction of the *x* axis), with values that decrease as the distance to tunnel wall decreases. It should be noted that no overpressure is observed in the numerical results. For the case with a *v/k* ratio equal to 7.3E5 (case 1.d.), a slight overpressure develops before the passage of the face and begins to dissipate before the face arrival. However, for the cases with higher *v/k* ratios (i.e. 1.5E6 to 1.5E7; cases 1.c to 1.a), an overpressure is observed at a distance up to about one radius from tunnel wall, in the direction of the *x* axis. The overpressure is higher for a higher ratio *v/k*. At a distance from the tunnel wall of about $0.2 \times D$, it is observed that an overpressure develops before the passage of the tunnel face and vanishes after.

As it can be observed, the pore pressure evolution presents three different patterns depending on the ratio t_c/t_p: (1) for $t_c/t_p < 1$, no overpressure is observed before the face arrival; (2) for $t_c/t_p \approx 1$, a slight overpressure is observed before the passage of the face and begins to dissipate before the face arrival; (3) for $t_c/t_p > 1$, the induced overpressure is observed before the passage of the tunnel face. A detailed discussion of these different types of pore pressure response is presented in the next section.

3.1.2. Pore pressure evolution observed before the passage of the tunnel face

In order to better understand the three-dimensional redistribution of stresses induced by the excavation in the near zone to tunnel face, Eberhardt [31] has shown that further insights could be gained by following a unit volume response as the tunnel face approaches it. To this aim, the pore pressure evolution at one point is followed as the tunnel face advances, until it arrives at a distance of about $0.2 \times D$. It should be noted that this distance has been chosen in order to be far enough of the corner that delimits tunnel face and tunnel wall. Fig. 4 shows the pore pressure evolution of four selected points located, in the direction of the x axis, at: the tunnel axis (A1), the tunnel wall (A2), $0.2 \times D$ (A3) and $0.5 \times D$ from tunnel wall (A4) (Fig. 2).

For a low value of v/k (Fig. 4d), the pore pressure evolution at point A2 presents a similar response as the one obtained on A1. For a larger value of v/k, the dissipation is slightly different. This difference observed can be linked to the rotation of the principal stress axes induced by the progressive advancement of the tunnel face advance [31]. Stress concentration in association with stress rotation close to the tunnel face influences ground deformation and thus, the pore pressure evolution.

Deeper in the rock, for points A3 and A4, it is observed that for a low value of v/k (Fig. 4d, $t_c/t_p < 1$), pore pressure changes occur at a distance of about $2 \times D$ ahead of the

tunnel face. Moreover, it is observed that the pore pressure diminishes as the distance to the tunnel wall decreases, as explained above. For a larger value of *v/k* (from 7.3E5 and higher), it is observed that the pore pressure begins to increase at about $2 \times D$ from the tunnel face and that higher overpressures are observed at higher values of *v/k*.

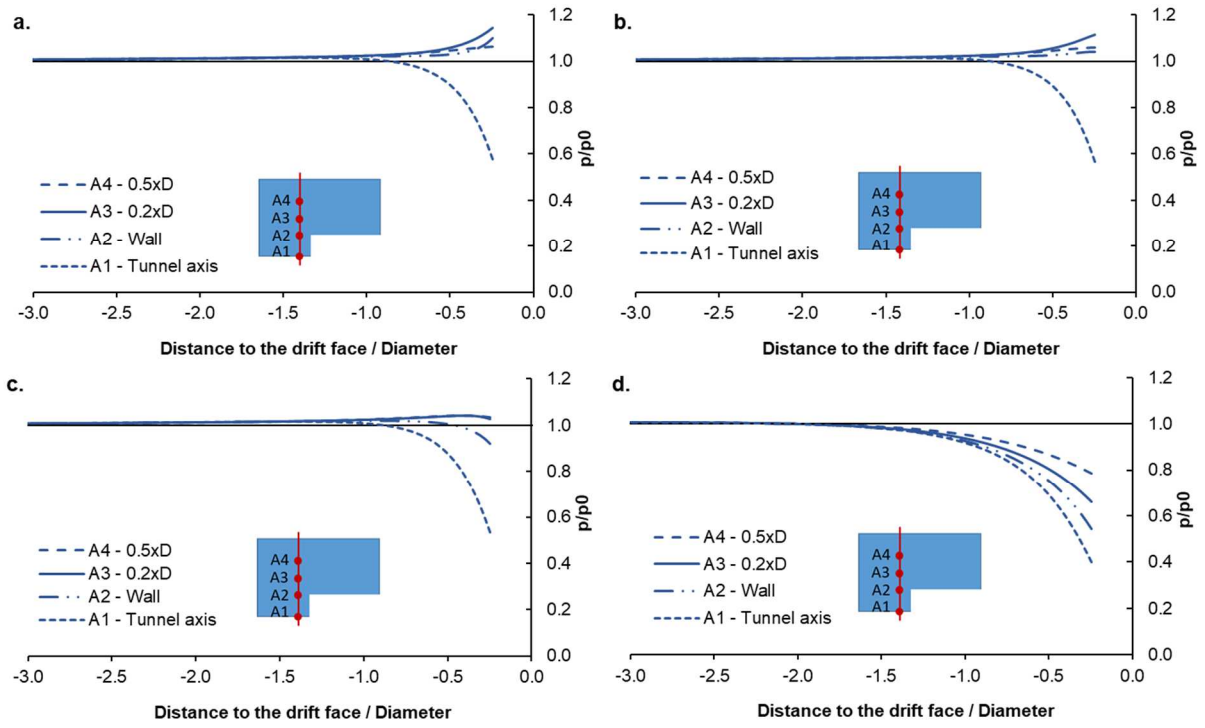

Fig. 4. Pore pressure evolution induced by tunnel advance. Four points located ahead of tunnel face at a distance of about $0.2 \times D$ are considered. Points are located on the *x* axis direction at: the tunnel axis (A1), the tunnel wall (A2), $0.2 \times D$ and $0.5 \times D$ from tunnel wall (A3 and A4). a. *v/k* = 1.5E7; b. *v/k* = 1.5E6; c. *v/k* = 7.3E5; d. *v/k* = 1.5E5.

As explained by Prassetyo and Gutierrez [27] this non-monotonic behavior and the increase of the pore pressure are related to the Mandel-Cryer effect [32-34], which is a consequence of the hydro-mechanical coupling. When the pore pressure at the tunnel boundary starts to dissipate, the induced local deformation may lead to an immediate effect inside the ground, leading to an increase of the pore pressure. Therefore, the induced pore pressure in the ground

ahead of the face increases above the initial pore pressure value before the face arrival. For cases with low values of the ratio t_c/t_p (<1), the pore pressure dissipates. However, for higher excavation rates (t_c/t_p >1), induced overpressures are observed even after the passage of the tunnel face.

Note that, before the passage of the tunnel face, the response obtained for cases with t_c/t_p >1 is similar to the undrained response. These results confirm that excavating in a ground with a very low permeability and/or high rate of excavation leads to a quasi-undrained response in the short-term. Appendix B presents a comparison of the results obtained for case 1.a. with a simulation performed by considering elastic undrained parameters. These results are in accordance with in-situ observations. As explained by Armand et al. [2] and Corkum et al. [35], if the advance rate is fast enough no excess pore pressure is dissipated; while with a low rate of excavation pore pressure diffuses and over-pressures are lower.

3.2. Anisotropic case – 3D model

As shown in several recent papers [e.g. 2, 6, 10, 35] field monitoring during the excavation progress in low permeability ground, as claystone, shows pore pressure changes around tunnels with overpressures induced by the face advance. It is observed that, the amplitude of the overpressure peak in the ground depends upon several factors, such as the orientation of the tunnel with the major principal stress, the distance to the tunnel wall and also the distance to the face. In order to study the influence of the anisotropy on the pore pressure evolution induced by the tunnel excavation, two additional cases are considered in the following:

Case 2: An isotropic initial stress state with an inherent anisotropy of the material;

Case 3: An anisotropic initial stress state, and an inherent anisotropy of the material.

A 3D finite element analysis is performed on a 104 m×80 m×80 m size model, considering the same radius of the tunnel as before (R = 2.6 m).

Fig. 5 shows the model geometry, the finite element mesh, and the initial and boundary conditions. The results presented in this analysis are obtained after 22 steps of excavation, corresponding to 52.8 m of excavation. Here again, a zero pore pressure is imposed at the tunnel wall. In order to compare the numerical results with field measurements, the elastic and hydraulic parameters considered for this simulation are based on the parameters proposed by Guayacán-Carrillo et al. [6] and are given in Table 3. An elastic transversely anisotropic behavior (E_x=E_z) is assumed for the rock mass.

Table 3. Elastic and hydraulic parameters considered in the 3D numerical model

Cases	$\sigma_{x,0}$ (MPa)	$\sigma_{y,0}$ (MPa)	E_x (MPa)	E_y (MPa)	v_{xz}	v_{yx}	k_x (m^2)	k_y (m^2)	ϕ_0
2	≈1.0 $\sigma_{y,0}$	12.4	6400	4000	0.2	0.3	2.7E-20		0.18
3.a.	≈1.3 $\sigma_{y,0}$	12.4	6400	4000	0.2	0.3	2.7E-20		0.18
3.b.	≈1.6 $\sigma_{y,0}$	12.4	6400	4000	0.2	0.3	2.7E-20		0.18

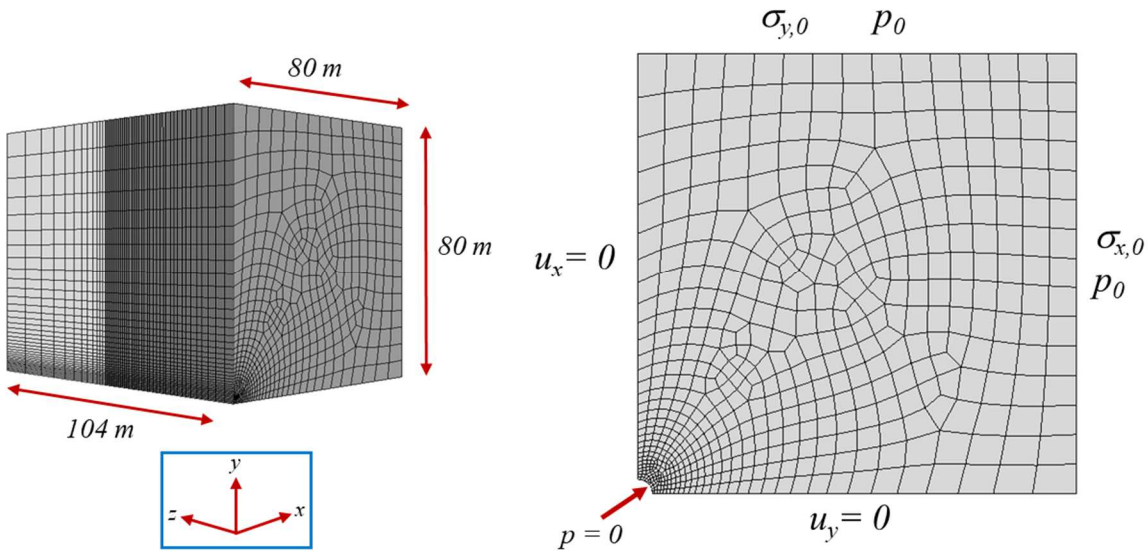

Fig. 5. Initial and boundary conditions for 3D numerical model ($\sigma_{x,0}$ and $\sigma_{y,0}$ are the initial stress state; and p_0 the initial pore pressure).

Fig. 6 shows different positions analyzed in the following. Note that points A1 to A4 are located at the same positions as in the axisymmetric model, presented in the section above.

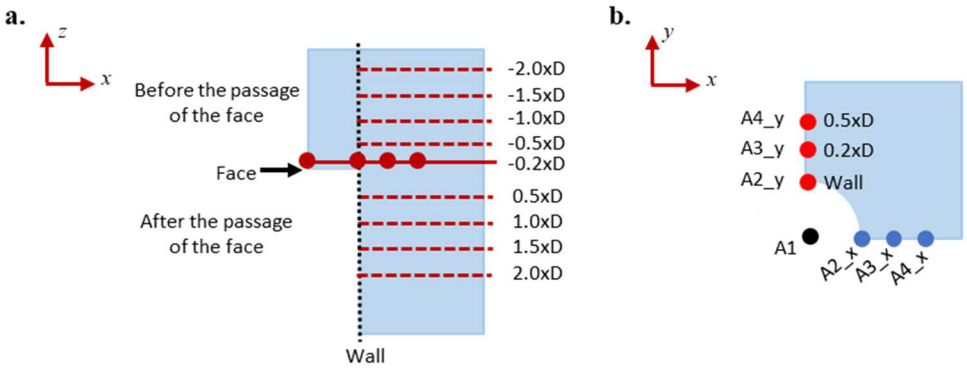

Fig. 6. Position of studied sections. a. In the plane *x*-*z*. In dashed lines, sections followed in the *x* axis direction. Sections are located from 2 diameters before to 2 diameters after the passage of the tunnel face. b. In the plane *x*-*y*. A1 to A4 are selected points located ahead of tunnel face, at a distance of about $0.2\times D$.

Fig. 7 shows the pore pressure evolution obtained for Case 2. In Fig. 7.a it is observed that the pore pressure evolution is very similar in the three points (A1, A2_x and A2_y) and that a difference is observed at a distance of about $0.6 \times D$, between the pore pressure evolution on point A1 as compared to the two other points. As explained in the above section, this difference is mainly related to the stress rotation induced by the progressive face advance. Moreover, a slight difference begins to be observed between the pore pressure evolution at points located on the axis of horizontal tunnel wall (A2_x) and on tunnel crown (A2_y). Note that for points located deeper in the rock (A4_x and A4_y, at around $0.5 \times D$ from tunnel

wall, Fig. 7.b a slight overpressure is also observed, mainly in the horizontal direction of the cross section (A4_x).

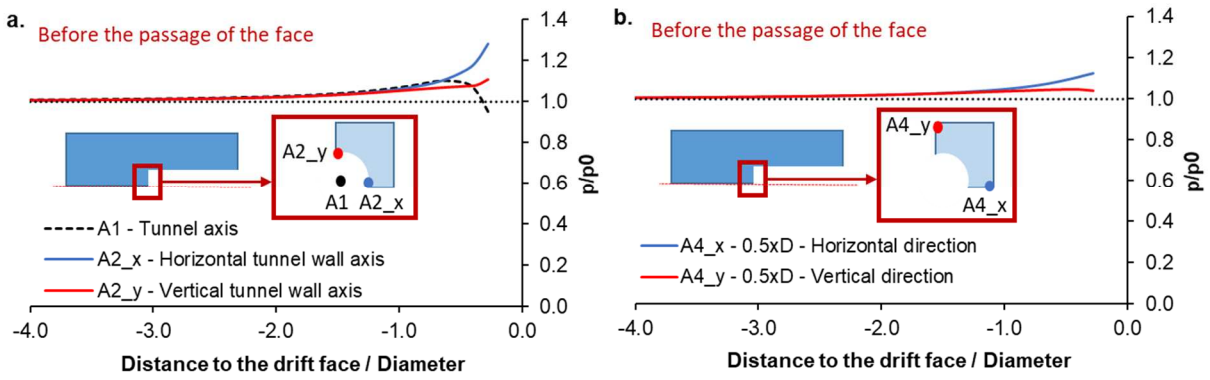

Fig. 7. Pore pressure evolution induced by tunnel advance. Plots refer to various selected points located ahead of tunnel face, at a distance of about $0.2 \times D$. a. In the tunnel axis (A1), the horizontal and the vertical tunnel wall axis (A2_x and A2_y); b. In the horizontal and the vertical direction of the cross section at $0.5 \times D$ from tunnel wall (A4_x and A4_y).

Comparing the pore pressure evolution obtained for Case 2 and Case 3 (a and b) it is observed that, along the tunnel axis (Fig. 8), the pore pressure changes before the passage of the tunnel face are observed on distances beyond 3 diameters. This is in accordance with the field observations in claystone formations [2-4,9], for which the excavation affects the pore pressure on a distance of about four diameters. Moreover, it is observed that the overpressure is stronger for an anisotropic initial stress state. For a higher anisotropy ratio of the initial stress state, a higher overpressure is obtained. For the studied cases, a maximum of about $1.10 \times p_0$ is obtained for case 2, $1.14 \times p_0$ for case 3.a. and $1.20 \times p_0$ for case 3.b.

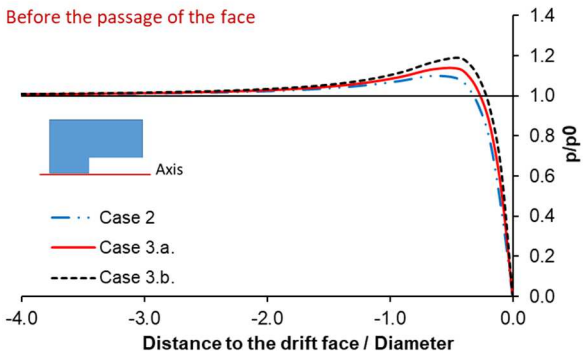

Fig. 8. Pore pressure evolution, at tunnel axis, induced by tunnel excavation in anisotropic medium with a ratio v/k = 1.5E7, before the passage of the tunnel face.

Looking at the pore pressure evolution before and after the passage of the face, it is observed that in both studied cases the pore pressure field is anisotropic. Overpressures are developed in the horizontal direction of the cross section, in the direction of the x axis. Fig. 9 presents isolines of the pore pressure field around the tunnel face. Fig. 10 presents the pore pressure evolution (in the direction of the x axis) induced by the tunnel excavation in an anisotropic medium with a ratio v/k = 1.5E7 (t_c/t_p >1), from 2 diameters before to 2 diameters after the passage of the tunnel face (Case 2 and Case 3.a.). It is observed that the overpressure is higher before the passage of the face in Case 3.a., while it is more pronounced after the passage of the face in Case 2. These observations suggest that, in addition to the ratio v/k, the anisotropy of the initial stress state has a significant effect on the pore pressure field before the passage of the tunnel face (i.e. when the deconfinement of the rock mass formation is still very weak), while after the passage of the face, the pore pressure response is mainly affected by the inherent anisotropy of the material.

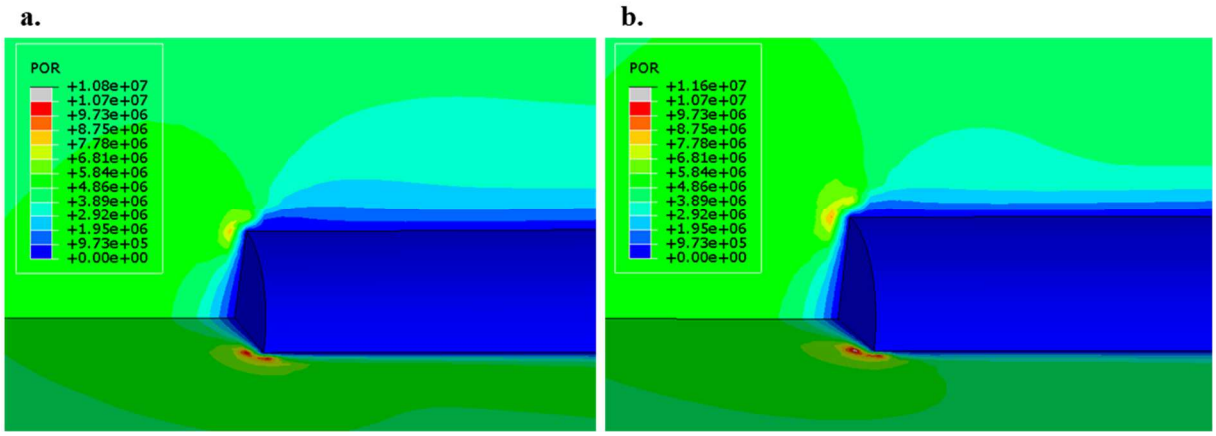

Fig. 9. Isolines of pore pressure field induced by tunnel excavation in anisotropic medium with a ratio *v/k* = 1.5E7, before and after the passage of the face. a. Case 2; b. Case 3.a.

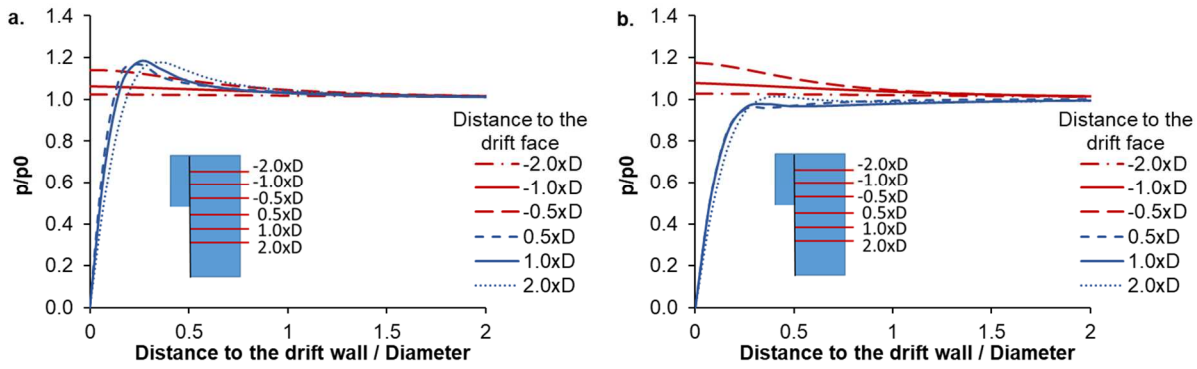

Fig. 10. Pore pressure evolution induced by tunnel excavation in anisotropic medium with a ratio *v/k* = 1.5E7, before and after the passage of the face. Pore pressure change at the horizontal direction of the cross section (at *x* axis direction). a. Case 2; b. Case 3.a.

3.3. Discussion of the results and comparison with in-situ measurements

Fig. 11 presents in-situ pore pressure measurements around experimental drifts excavated in Callovo-Oxfordian claystone [6]. It should be noted that the boreholes devoted to the pore pressure measurements have been installed before the beginning of the drift excavation as a part of mine-by-tests [6, 8]. Therefore, boreholes permit to follow the pore pressure evolution induced by the excavation progress. In-situ measurements have shown an anisotropic pore

pressure distribution around experimental drifts, which depends on the drifts orientations. For drifts following the direction of σ_H (similar to Case 2 in this work), overpressures in the horizontal direction (i.e. in the direction of the *x* axis) have been measured before the passage of the face. The pore pressure drops down at the vicinity of the drift wall when the drift's face passes by the monitored section. After the passage of the face, an overpressure is observed inside the rock, with a maximum overpressure situated at about 1–1.5 diameters from the drift wall [2,6]. In-situ observations do not show a significant overpressure in the vertical direction. For drifts following the direction of σ_h (similar to Case 3.a.), an overpressure in the lateral direction has also been recorded before the face passage. Higher values of overpressures are observed for drifts excavated following the direction of σ_H [2, 5, 6, 36].

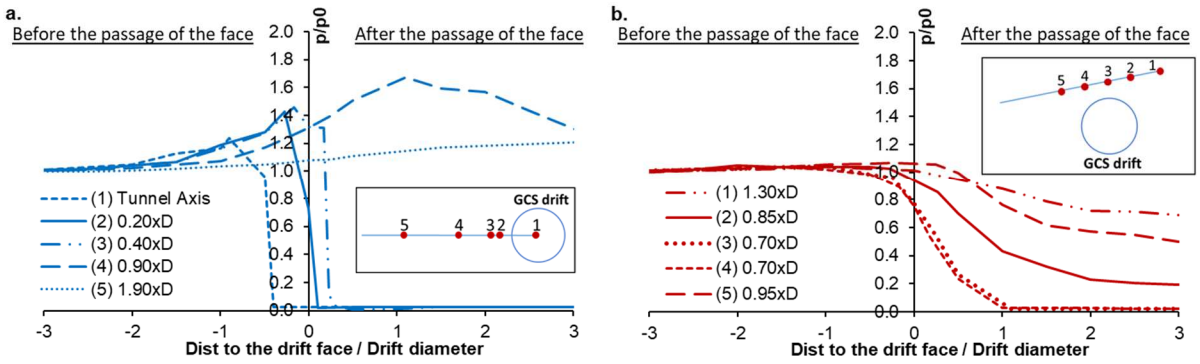

Fig. 11. Measurements recorded during GCS drift excavation at M/HM URL. Pore pressure evolution in the horizontal (a.) and vertical (b.) direction of the cross section. D – drift diameter (adapted from Guayacán-Carrillo et al. [6]).

Comparing with numerical results, it is observed that poroelastic analysis allows to describe some main trends observed in-situ:

- The numerical results allow to reproduce pore pressure changes before the passage of the face. Pore pressure increase before the passage of the tunnel face is observed on distances beyond 3 diameters.

- For both cases (i.e. Case 2 and Case 3.a), an overpressure is obtained in the horizontal direction of the cross section. This overpressure is observed before the passage of tunnel face. After the passage of the tunnel face, an overpressure is observed in the results obtained for the Case 2. It is important to note that Guayacán-Carrillo et al. [6] based on a 2D poroelastic model has studied the influence of the anisotropy of the elastic moduli. To this aim different anisotropy ratios (E_x/E_y) from 1.2 to 2.0 have been considered. It has been observed that, for similar parameters to the ones of Case 2, an overpressure is always obtained in the horizontal direction (as recorded in-situ). While, for similar parameters as to the ones of Case 3.a., an overpressure in the horizontal direction of the drift cross section is obtained only for an anisotropy ratio of the Young's modulus (E_x/E_y) greater than about 1.4. For a higher anisotropy ratio of the Young's modulus, higher overpressures are obtained in the horizontal direction.
- In-situ observations have shown that the pore pressure evolution is very similar for different drift sizes (diameter of 0.9 m, 5 m and 9 m [2, 36]). As explained by Vu et al. [5], some differences between these excavations are observed in terms of magnitude near the drift wall. The rate of excavation also plays a role at it is higher for micro-tunnels (i.e. 0.9 m of diameter). Induced overpressures are observed before the passage of the face, with higher overpressure values at higher values of v/k, which is in accordance with results presented in section 3.1.

In summary, based on the performed poroelastic analysis, it is observed that overpressures can be induced: (1) before the passage of the face, depending on the anisotropy of the initial stress state and on the interplay between the excavation rate and the permeability of the rock mass formation; (2) after the passage of the face, anisotropic pore pressure field is mainly related to the anisotropy of the elastic stiffness of the ground.

Note that, the in-situ measured overpressures have reached higher values than the ones obtained in the numerical simulations. Moreover, the maximum measured overpressure is situated at a deeper distance to the tunnel wall than the one obtained in the numerical results. In fact, as observed in the field and discussed in the literature [e.g. 12, 31], rock will yield under high stresses, resulting in stress redistribution and dilatancy around the tunnel and near the face. Therefore, it is expected that pore pressure will decrease in a zone close to the tunnel wall. Notwithstanding, in-situ measurements have shown an overpressure deeper in the rock which could be related to the transversal isotropy [2, 5, 6]. As explained by Vu et al. [5], the anisotropic pore pressure field is related to the inherent anisotropy of the elastic stiffness and also to the anisotropy of the induced excavation damaged zone.

It is interesting to point out that, similar observations have been performed for excavations in Boom clay and Opalinus clay formations [e.g. 3,10]. Wild et al. [12], based on an experimental work studying the influence of the stress path on the hydro-mechanical response of the Opalinus clay, concluded that an increase in pore pressure as the tunnel face approaches the monitoring sensor location can be related to poroelastic response. As explained by Wild et al. [12], considering a tunnel excavated in a transversely isotropic medium and with an isotropic stress state, the stability is affected by the anisotropy of the medium. They also concluded that the different pore pressure evolutions related to transversal isotropy affects the state of failure of the rock mass around the excavation.

Drop in pore pressure in the nearest zone to the tunnel is not reproduced by this analysis, due to the simplified constitutive model used here. Failure and the associated stress drop will be studied in future work. The effect of non-linear and time dependent behavior of the rock mass as well as the effect of the anisotropic fractures network around the excavation

might significantly influence the evolution of the pore pressure field and will be addressed in future work.

4. Analysis of the face advance effect – from a 3D to a 2D model

Recent studies have been carried out on pore pressure evolution induced by excavation in a poro-elastoplastic ground. In an attempt to take into account the pore pressure evolution in a 2D model, Callari [26], and Callari and Casini [37] proposed a linear function of pore pressure vs. excavation time for tunneling in saturated ground. More recent works [27,38] have proposed a pore pressure evolution profile, taking into account the transient coupling effect between the fluid flow and the deformation induced by the excavation. However, the current practice for the simulation tunnels excavation in low permeability ground, as claystone, assumes a linear dissipation of pore pressure very close to tunnel face (e.g. [5,14,16,39]).

In order to better understand and reproduce the induced pore pressure variations in low permeability anisotropic ground, a simple poroelastic approach is proposed in this section. An analysis is performed based in a near section to tunnel wall ($0.2 \times D$). Fig. 12 presents the deconfinement rate and the pore pressure evolution for the case 1.a ($t_c/t_p > 1$), which is compared with cases 1.d ($t_c/t_p \approx 1$) and 1.e. ($t_c/t_p < 1$). For ratios $t_c/t_p \approx 1$ and $t_c/t_p > 1$, a pore pressure increase is observed before the passage of the face and is stronger for higher v/k ratios. Moreover, it is observed that a higher v/k ratio leads to delay the pore pressure dissipation. The excavation time remains very small as compared to the consolidation time. Therefore, the ground response close to the tunnel face can be identified to an undrained behavior, as explained above. Moreover, it is observed that this ratio affects the displacements evolution. Pore pressure increase will lead to a slight reduction of displacements, then displacements will increase as pore pressure dissipates.

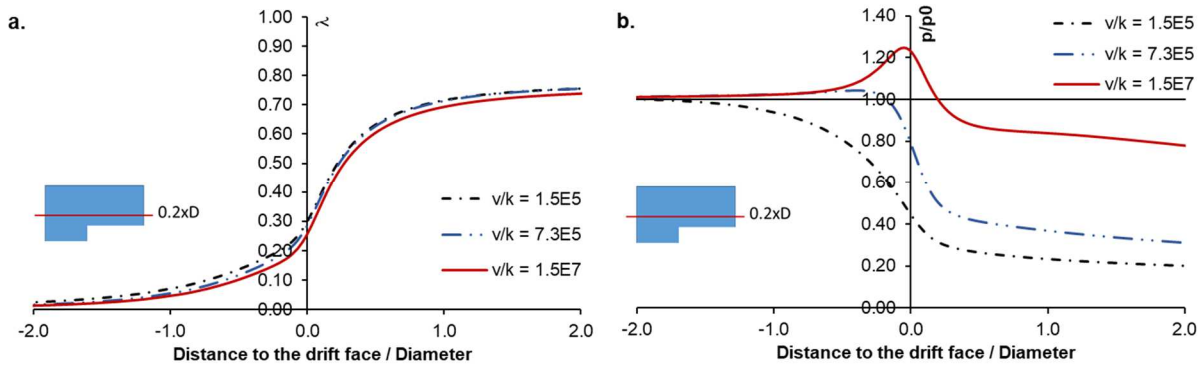

Fig. 12. Pore pressure evolution induced by tunnel excavation in an isotropic elastic medium with a ratio v/k = 1.5E5 ($t_c/t_p < 1$); v/k = 7.3E5 ($t_c/t_p \approx 1$); v/k = 1.5E7 ($t_c/t_p > 1$). a. Deconfinement rate curves. b. Pore pressure evolution (p/p_0).

For the isotropic case, as shown in Fig. 12, the first pore pressure changes are observed at about -2D (x_0) ahead of the tunnel face. Then, after the passage of the face, a strong pore pressure change is observed until about 1D. Afterwards, the pore pressure evolution is mainly related to the dissipation time. Thus, the excavation time can be defined as $t_p = 3D/v$ and the ratio t_c/t_p is given by $t_c/t_p = vL^2/(3DC_v)$.

In an attempt to better understand the influence of the pore pressure evolution condition in a 2D model, for low permeability ground, two simulations are proposed and compared considering the parameters of Case 1.a. Two different relations of pore pressure evolution are presented in Fig. 13. The first one, proposes a linear dissipation of pore pressure near to tunnel face. The second one, based on the analysis proposed by Prassetyo and Gutierrez [27] takes into account the transient coupling effect between fluid flow and deformation. For this purpose, before the passage of tunnel face, the pore pressure evolution is taken as the one obtained in undrained conditions. A slight overpressure begins to develop from $-2 \times D$, then the overpressure increases rapidly from $-0.5 \times D$ to the tunnel face. After the passage of the

face, the pore pressure strongly decreases until $0.5 \times D$ and then more slowly until $p/p_0 = 0$, when the tunnel face is at about $1 \times D$ and beyond.

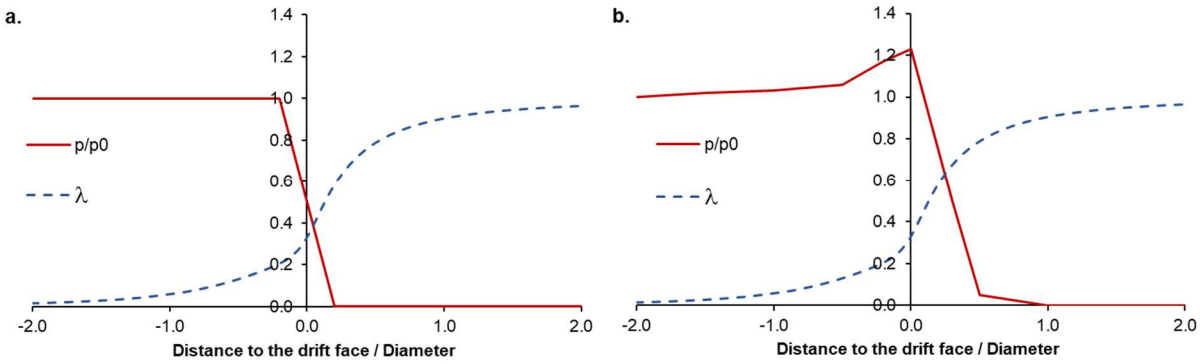

Fig. 13. Evolution of confinement ratio λ and of the pore pressure at the tunnel wall. a. Linear pore pressure dissipation very close to tunnel face. b. Pore pressure evolution taking into account the transient coupling effect between fluid flow and deformation.

Fig. 14 presents the pore pressure evolution obtained for an isotropic case by imposing a non-linear pore pressure evolution (Fig. 13b). Results show that the pore pressure increase before the passage of the tunnel face can be reproduced, however the overpressure remains very close to the wall. Indeed, for an isotropic 2D simulation, overpressures are not expected to occur. In this case the obtained overpressure is mainly controlled by the imposed pore pressure at the tunnel wall.

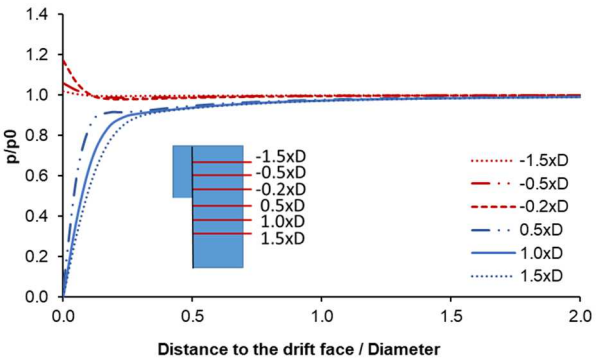

Fig. 14. Horizontal pore pressure evolution induced by tunnel excavation in isotropic medium with a ratio v/k = 1.5E7, before and after the passage of the face.

Accounting for an equivalent isotropic pore pressure rate, a simulation is performed using Case 2 parameters (isotropic initial stress state, and an inherent anisotropy of the material). Thus, pore pressure rates proposed in Fig. 13 are used. Note that, Case 1.a and Case 2 present similar initial conditions. The elastic parameters values of Case 1.a. are the average parameters values of Case 2.

Fig. 15 presents the pore pressure evolution in the horizontal direction (i.e. in the direction of the x axis) obtained by imposing the two different pore pressure profiles. It is observed that taking into account pore pressure increase ahead of tunnel face, permits a better reproduction of the pore pressure in time, as compared to 3D results presented in previous sections. Before the passage of the face, for both cases, an increase of the pore pressure is observed inside the rock up to $0.5 \times D$ from tunnel wall (i.e. in the direction of the x axis). However, for the case with linear dissipation this increase remains weak. After the passage of the tunnel face, pore pressure dissipates slower for the case with non-linear pore pressure rate.

It is observed that for low permeability ground, overpressures induced before the passage of the face can be reproduced in a 2D model by taking into account an undrained ground response. After the passage of the face, taking into account a transient response will lead to a better reproduction of the pore pressure evolution in time. This response is mainly influenced by face advance rate and ground consolidation time. Higher pore pressure values can be observed in the zone close to the tunnel face.

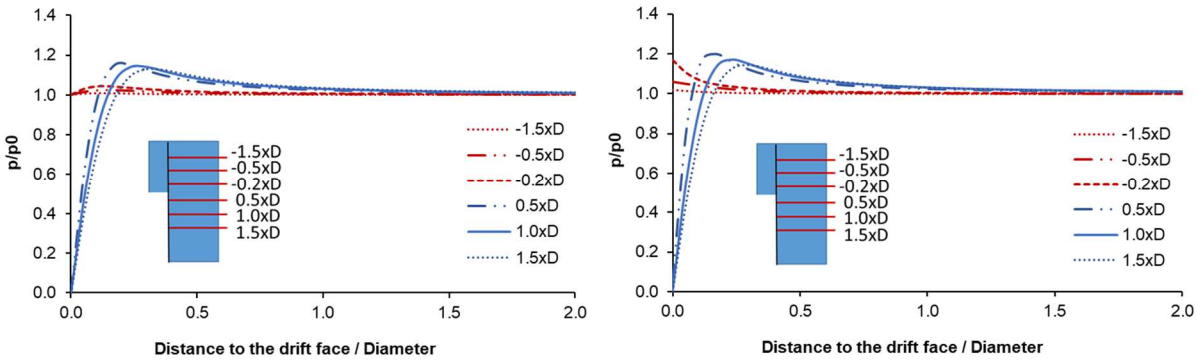

Fig. 15. Horizontal pore pressure evolution induced by tunnel excavation in anisotropic medium with a ratio *v/k* = 1.5E7, before and after the passage of the face. Left side: linear pore pressure rate; right side: non-linear pore pressure rate.

5. Conclusions

Pore pressure evolution induced by excavation of tunnels in low permeability anisotropic ground is investigated using a 3D fully coupled hydro-mechanical finite element simulation. An analysis has been performed by taking into account different features that can influence the pore pressure evolution around tunnel excavation such as: the excavation rate, the permeability of the ground, the anisotropy of the material and of the initial stress state.

First, special emphasis is given to the influence of face advance in an isotropic ground. The obtained numerical results show that the pore pressure evolution depends on the interplay between the excavation rate and the ground consolidation time. Indeed, for rapid excavation rate with respect to the consolidation time, the ground response close to the tunnel face can be considered as undrained. Overpressures are obtained before the passage of the tunnel face.

Subsequently, an analysis of the impact of anisotropic initial stress state and mechanical anisotropy of the rock was performed. The obtained numerical results have evidenced that overpressures can be induced before the passage of the face, depending on the anisotropy of the initial stress state and on the interplay between excavation rate and consolidation time of

the rock mass formation. After the passage of the face, the anisotropy of the pore pressure response is mainly related to the anisotropy of the elastic stiffness of the ground.

Finally, in an attempt to propose a pore pressure evolution at the tunnel wall that can be used in 2D models of tunnel excavation, an analysis of the pore pressure evolution at tunnel wall is presented. It is observed that for low permeability ground, overpressures induced before the passage of the face can be reproduced in a 2D model by assuming an undrained response of the ground. After the passage of the face, taking into account a transient response between tunnel face and 1 diameter behind this one, leads to a good reproduction of the pore pressure evolution in time as compared to 3D numerical simulations.

Comparison with in-situ measurements has shown that the main trends of the pore pressure evolution can be simulated and analyzed based on an efficient and simplified poroelastic model. In-situ pore pressure evolution, mainly the observed overpressure, will play a key role in the failure initiation and development around excavations. Further quantification of these mechanisms is required to move towards a comprehensive model that also accounts for non-linear behavior of the porous material and failure initiation and propagation. In the future, this work will be extended by introducing a degradation of the rock properties and an increase of the permeability in zones where the failure criterion is reached.

Appendix A – Mesh validation

The geometry of the model exhibits a sharp corner at the intersection between the face and the tunnel wall. As explained in the literature domains with reentrant corners could present a global loss of accuracy caused by the influence of the singularity point. Several approaches are used to improve the accuracy of the solution in the zone around corner, most of them showed that accuracy of solution near the singularity can be improved by a graded mesh

refinement towards singularity point (e.g. [40, 41]). Therefore, in practice the most common approaches are based in systematic local mesh refinement near the singularities.

Moreover, for analysis of coupled solid-fluid problems within the finite element method, mixed element formulations are used for the spatial discretization, where stable discretization is to use quadratic shape functions for the solid displacement and linear shape functions for the pressure [42, 43]. Mesh elements characterized by 8-node biquadratic displacement, bilinear pore pressure interpolation have been used.

In order to analyze the singularity influence on results, several numerical simulations have been performed by a procedure of graded mesh refinement towards the corner. Fig. A.1 presents the evolution of hoop stress and Fig. A.2 the pore pressure evolution for three different mesh coarseness. It is observed that the influence zone of the singularity around the corner is reduced with refinement mesh and remains very close to the corner. At a distance of about $0.2 \times D$ it is observed that pore pressure evolution is similar between three models.

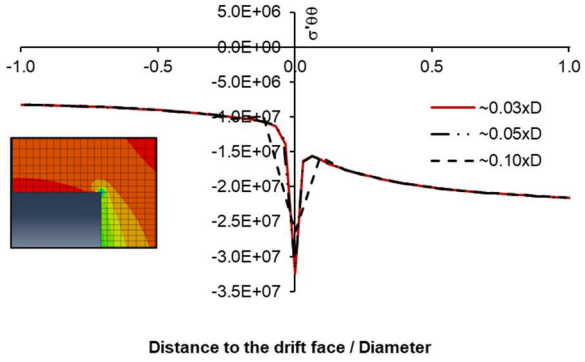

Fig. A.1. Hoop effective stress ($\sigma'_{\theta\theta}$) at tunnel wall obtained from simulation of an excavation with drained boundary conditions. Mesh size variations from 0.03xD to 0.10xD.

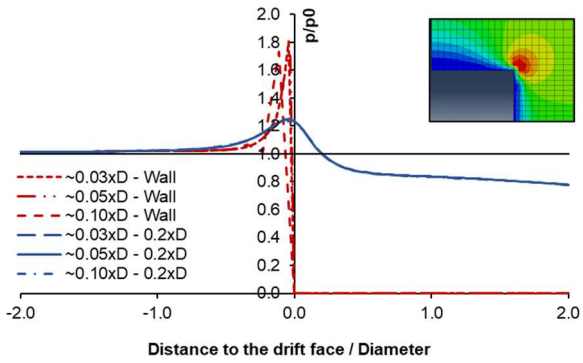

Fig. A.2. Pore pressure evolution obtained from simulation of an excavation with drained boundary conditions. Results obtained at tunnel wall and at a distance of $0.2 \times D$ from tunnel wall. Mesh size variations from 0.03xD to 0.10xD.

Appendix B – Pore pressure evolution obtained from undrained case

Based on the set of parameters obtained from laboratory work by Braun et al. [44], the undrained elastic parameters considered for this simulation are presented in Table B.1. Fig. B.1 presents a comparison of obtained results with Case 1.a. (drained case). The pore pressure evolution before the passage of the tunnel face is shown at four different points, located on the x axis direction at: the tunnel axis (A1), the tunnel wall (A2), $0.2 \times D$ from tunnel wall (A3) and $0.5 \times D$ from tunnel wall (A4). Note that this simulation is performed in terms of total stresses and strain by solving the purely mechanical problem using undrained properties of the ground. Then, the pore pressure field is calculated from the computed strain field. The pore pressure change can be expressed as $\mathrm{d}p = -Mb_{ij}\mathrm{d}\varepsilon_{ij}$, where M is the Biot undrained modulus and b_{ij} the Biot effective stress coefficient tensor.

Table B.1. Elastic undrained mechanical parameters

Cases	$\sigma_{x,0}$ (MPa)	$\sigma_{y,0}$ (MPa)	E_u (MPa)	v_u
1	12.4		8500	0.35

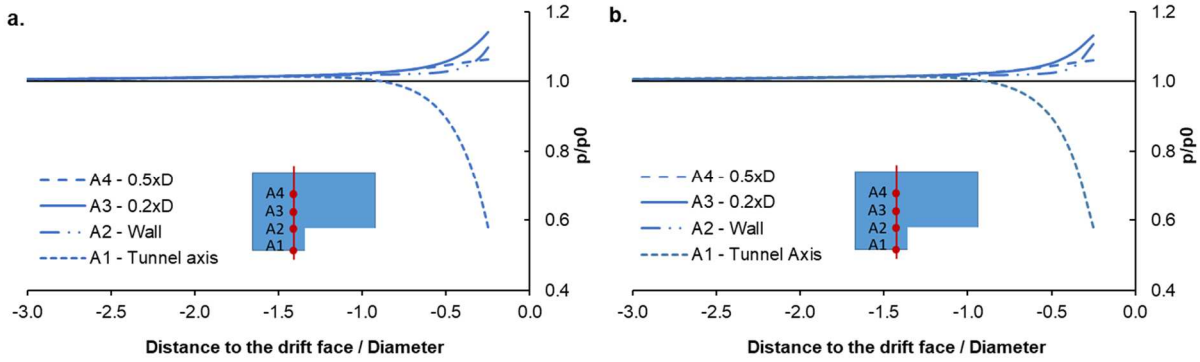

Fig. B.1. Evolution of pore pressure before passage of the tunnel face. a. Results from Case 1.a. b. Model taking into account undrained elastic parameters. Four points located ahead of tunnel face at a distance of about $0.2 \times D$ are followed. Points are located, in the direction of the x axis, at: tunnel axis (A1), tunnel wall (A2), $0.2 \times D$ and $0.5 \times D$ from tunnel wall (A3 and A4).

6. References

[1] Corkum AG, Martin CD. Modelling a mine-by test at the Mont Terri rock laboratory, Switzerland. Int J Rock Mech Min Sci 2007; 44:846–859. https://doi:10.1016/j.ijrmms.2006.12.003.

[2] Armand G, Noiret A, Morel J, Seyedi DM. Pore pressure change during the excavation of deep tunnels in the Callovo-Oxfordian claystone. In: Proc. of 13th ISRM Congress. Montreal; 10-13 May 2015. 13 p. ISBN: 978-1-926872-25-4.

[3] Vaunat J, Gens A, De Vasconcelos R . Anisotropic effects in a deep excavation in stiff clays. In: Computational plasticity XII: Fundamentals and applications – Proc. of the 12th Int Conf on Computational Plasticity, COMPLAS 2013, Barcelona, Spain, September 2013, 8p.

[4] Giger SB, Marschall P, Lanyon B, Martin CD. Hydromechanical response of Opalinus clay during excavation works – A synopsis from the Mont Terri URL. In: Schubert & Kluckner (Eds.), Future development of Rock Mechanics, Proc. ISRM regional symposium Eurock 2015 & 64th Geomechanics colloquium. Salzburg, October 2015, p. 609-614. ISBN 978-3-9503898-1-4.

[5] Vu MN, Guayacán-Carrillo LM, Armand G. Excavation induced over pore pressure around a drift in Callovo-Oxfordian claystone. Eur J Env Civil Eng 2020. doi: 10.1080/19648189.2020.1784800.

[6] Guayacán-Carrillo LM, Ghabezloo S, Sulem J, Seyedi DM, Armand G. Effect of anisotropy and hydro-mechanical couplings on pore pressure evolution during tunnel excavation in low-permeability ground. Int J Rock Mech Min Sci 2017; 97:1-14. https://doi:10.1016/j.ijrmms.2017.02.016.

[7] Marschall P, Trick T, Lanyon GW, Delay J, Shao H. Hydro-Mechanical Evolution of Damaged Zones around a Microtunnel in a Claystone Formation of the Swiss Jura Mountains. Conference paper, 42nd US Rock Mechanics Symposium and 2nd US – Canada Rock Mechanics symposium, San Francisco, June 29 – July 2, 2008, 11 p.

[8] Noiret A, Armand G, Cruchaudet M & Conil N (2011). Mine-by experiments in order to study the hydromechanical behavior of the Callovo-Oxfordian claystone at the Meuse Haute-Marne underground research laboratory (France). Proc. 8th Int symposium on field measurements in geomechanics, FMGM. Berlin, Sept 2011, p. 12–16.

[9] Armand G, Noiret A, Cruchaudet M, Conil N. Mine by experiment performed in the Callovo-Oxfordian Claystone at the Meuse Haute Marne underground research laboratory

(France). In: Q. Qian & Y. Zhou (eds), Harmonising Rock Engineering and the Environment, Proc. 12th ISRM Congress. Beijing, Oct 2011, p. 157-162.

[10] Wild KM, Amann F, Martin CD. Some fundamental hydro-mechanical processes relevant for understanding the pore pressure response around excavations in low permeable clay rocks. ISRM Congress 2015 Proceedings - 13th Int Congr Rock Mech, 10-13 May 2015, Montreal, Canada, e505.

[11] Wild KM and Amann F. Experimental study of the hydro-mechanical response of Opalinus Clay – Part 1: Pore pressure response and effective geomechanical properties under consideration of confinement and anisotropy. Eng Geol 2018; 237:32-41.

[12] Wild KM and Amann F. Experimental study of the hydro-mechanical response of Opalinus Clay – Part 2: Influence of the stress path on the pore pressure response. Eng Geol 2018; 237:92-101.

[13] Coarita-Tintaya ED, Souley M, Vu MN, Golfier, F. Numerical Anisotropic modelling of a deep drift ah the Meuse/Haute-Marne URL. Fourth International Symposium on Computational Geomechanics (ComGeo IV), Assisi, Italy. 2-4 May, 2018.

[14] Coarita-Tintaya ED, Golfier F, Souley M, Vu MN. Anisotropic hydro-viscoplastic modelling of a drift at the Meuse/Haute-Marne URL. Eur J Env Civil Eng 2020. doi: 10.1080/19648189.2020.1797887.

[15] Manica M, Gens A, Vaunat J, Ruiz DF. A time-dependent anisotropic model for argillaceous rocks. Application to an underground excavation in Callovo-Oxfordian claystone. Comput Geotech 2017; 85:341–350.

[16] Pardoen B, Levasseur S, Collin F. Using local second gradient model and shear strain localisation to model the Excavation Damaged Zone in unsaturated Claystone. Rock Mech Rock Eng 2015; 48:691-714. https://doi:10.1007/s00603-014-0580-2.

[17] Salehnia F, Collin F, Li XL, Dizier A, Sillen X, Charlier R. Coupled modeling of Excavation Damaged Zone in Boom clay: Strain localization in rock and distribution of contact pressure on the gallery's lining. Comput Geotechnics 2015; 69:396–410. https://doi:10.1016/j.compgeo.2015.06.003.

[18] Coussy O. Poromechanics. John Wiley & Sons, Chichester; 2004.

[19] Detournay E, Cheng A HD. Fundamentals of Poroelasticity. In: C. Fairhurst, Editor. Comprehensive Rock Engineering: Principles, Practice and Projects. Vol. II, Analysis and Design Method, Pergamon Press; 1993, p. 113-171.

[20] Biot MA. General theory for three-dimensional consolidation. J Appl Phys 1941; 12:155-164.

[21] Biot MA, Willis DG. The elastic coefficients of the theory of consolidation. J Appl Mech 1957; 24:594-601.

[22] Berryman J. Effective stress for transport properties of inhomogeneous porous rock. J Geophys Res 1992; 97:17409–17424.

[23] Ghabezloo S, Sulem J, Guédon S, Martineau F, Saint-Marc J. Poromechanical behaviour of hardened cement paste under isotropic loading. Cem Concr Res 2008; 38:1424–1437.

[24] Giraud A, Rousset G. Time-dependent behaviour of deep clays. Eng Geology 1996; 41:181–195. https://doi.org/10.1016/0013-7952(95)00000-3

[25] Li X. Stress and displacement fields around a deep circular tunnel with partial sealing. Comput Geotech 1999, 24:125–140.

[26] Callari C. Coupled numerical analysis of strain localization induced by shallow tunnels in saturated soils. Comput Geotech 2004; 31:193–207.

[27] Prassetyo SH, Gutierrez M. Effect of transient coupled hydro-mechanical response on the longitudinal displacement profile of deep tunnels in saturated ground. Tunn Undergr Sp Technol 2018; 75:11–20. https://doi.org/10.1016/j.tust.2018.02.003.

[28] Ghabezloo S, Sulem J, Saint-Marc J. Evaluation of a permeability-porosity relationship in a low-permeability creeping material using a single transient test. Int J Rock Mech Min Sci 2009; 46:761–768. https://doi.org/10.1016/j.ijrmms.2008.10.003.

[29] Belmokhtar M, Delage P, Ghabezloo S, Tang AM, Menaceur H, Conil N. Poroelasticity of the Callovo-Oxfordian claystone. Rock Mech Rock Eng 2016; 50:871-889. https://dx.doi.org/10.1007/s00603-016-1137-3.

[30] Anagnostou G. The one-step solution of the advancing tunnel heading problem. In: Eberhardsteiner J. et al., editors. ECCOMAS Thematic conference on Computational Methods in Tunneling. Vienna, Austria, August 2007, 17 p.

[31] Eberhardt, E. Numerical modelling of three-dimension stress rotation ahead of an advancing tunnel face. Int J Rock Mech Min Sci 2001; 38:499–518. https://doi:10.1016/S1365-1609(01)00017-X.

[32] Mandel J. Consolidation des sols (étude mathématique). Géotech 1953; 3:287-299.

[33] Cryer CW. A comparison of the three-dimensional consolidation theories of biot and terzaghi. Q J Mech Appl Math 1963; 16:401–412. https://doi.org/10.1093/qjmam/16.4.401.

[34] Verruijt A. Theory and problems of poroelasticity. Delft University of Technology; 2013.

[35] Corkum, AG. A Model for Pore Pressure Response of a Claystone due to Liberated Residual Stress Dilation. Rock Mech Rock Eng 2020, 53(2): 587–600. doi:10.1007/s00603-019-01938-x.

[36] Guayacán-Carrillo LM, Armand G, Conil N, de la Vaissière R, Djizanne H. Impact of size excavation on time-dependent behavior of drifts excavated at the Meuse/Haute-Marne URL. Proc. 14th Int Congress Rock Mech Rock Eng (ISRM 2019), p. 686 – 692.

[37] Callari C, Casini S. Tunnels in saturated elasto-plastic soils: three-dimensional validation of a plane simulation procedure. In: Marceri F, Frémond M, editors. Mechanical Modelling and Computational Issues in Civil Engineering. Springer, Berlin; 2005, p. 143–164.

[38] Prassetyo SH, Gutierrez M. Effect of surface loading on the hydro-mechanical response of a tunnel in saturated ground. Undergr Sp 2016, 1:1–19. https://doi.org/10.1016/j.undsp.2016.06.001.

[39] Seyedi, DM, Armand G, Noiret A. "Transverse Action" – A model benchmak exercise for numerical analysis of the Callovo-Oxfordian claystone hydromechanical response to excavation operations. Comput Geotech 2017, 85:287-305.

[40] Apel T, Sändig AM, Whiteman JR. Graded mesh refinement and error estimates for finite element solutions of elliptic boundary value problems in non-smooth domains. Math Methods Appl Sci 1996; 19:63–85.

[41] Nguyen-Xuan H, Liu GR, Bordas S, Natarajan S, Rabczuk T. An adaptive singular ES-FEM for mechanics problems with singular field of arbitrary order. Comput Methods Appl Mech Eng 2013; 253:252–273. https://doi.org/10.1016/j.cma.2012.07.017.

[42] Brezzi F, Falk RS. Stability of higher-order hood-taylor methods. SIAM J Numer. Anal 1991; 28:581–590.

[43] Ehlers W, Ammann M, Diebels S. H-adaptive FE methods applied to single- and multiphase problems. Int J Num Methods Eng 2002; 54:219–239.

[44] Braun P, Ghabezloo S, Delage P, Sulem J, Conil N. Transversely isotropic poroelastic behaviour of the Callovo-Oxfordian claystone: A set of stress-dependent parameters. Rock Mech Rock Eng 2020 (Submitted).

Tables captions

Table 1. Elastic mechanical and hydraulic parameters

Table 2. Summary of different studied cases

Table 3. Elastic and hydraulic parameters considered in the 3D numerical model

Table B.1. Elastic undrained mechanical parameters

Figures captions

Fig. 1. Initial and boundary conditions for an axisymmetric model ($\sigma_{x,0}$ and $\sigma_{y,0}$ are the initial horizontal and vertical stresses and p_0 is the initial pore pressure).

Fig. 2. Position of the studied sections. In dashed lines, sections followed at different distances on x axis (distances are given with respect to the tunnel wall). Points A1 to A4 are selected points located ahead of tunnel face, at a distance of $0.2 \times D$ (D is the tunnel diameter).

Fig. 3. Pore pressure evolution induced by tunnel excavation in an isotropic elastic medium with a ratio v/k = 1.5E5 to 1.5E7. Sections located on the x axis at: a. In the axis of excavation; b. At $0.2 \times D$ from the tunnel wall; c. At one radius ($0.5 \times D$) from the tunnel wall; d. At one diameter (D) from the tunnel wall.

Fig. 4. Pore pressure evolution induced by tunnel advance. Four points located ahead of tunnel face at a distance of about $0.2 \times D$ are considered. Points are located on the x axis direction at: the tunnel axis (A1), the tunnel wall (A2), $0.2 \times D$ and $0.5 \times D$ from tunnel wall (A3 and A4). a. v/k = 1.5E7; b. v/k = 1.5E6; c. v/k = 7.3E5; d. v/k = 1.5E5.

Fig. 5. Initial and boundary conditions for 3D numerical model ($\sigma_{x,0}$ and $\sigma_{y,0}$ are the initial stress state; and p_0 the initial pore pressure).

Fig. 6. Position of studied sections. a. In the plane x-z. In dashed lines, sections followed in the x axis direction. Sections are located from 2 diameters before to 2 diameters after the passage of the tunnel face. b. In the plane x-y. A1 to A4 are selected points located ahead of tunnel face, at a distance of about $0.2 \times D$.

Fig. 7. Pore pressure evolution induced by tunnel advance. Plots refer to various selected points located ahead of tunnel face, at a distance of about $0.2 \times D$. a. In the tunnel axis (A1), the horizontal and the vertical tunnel wall axis (A2_x and A2_y); b. In the horizontal and the vertical direction of the cross section at $0.5 \times D$ from tunnel wall (A4_x and A4_y).

Fig. 8. Pore pressure evolution, at tunnel axis, induced by tunnel excavation in anisotropic medium with a ratio v/k = 1.5E7, before the passage of the tunnel face.

Fig. 9. Isolines of pore pressure field induced by tunnel excavation in anisotropic medium with a ratio v/k = 1.5E7, before and after the passage of the face. a. Case 2; b. Case 3.a.

Fig. 10. Pore pressure evolution induced by tunnel excavation in anisotropic medium with a ratio v/k = 1.5E7, before and after the passage of the face. Pore pressure change at the horizontal direction of the cross section (at x axis direction). a. Case 2; b. Case 3.a.

Fig. 11. Measurements recorded during GCS drift excavation at M/HM URL. Pore pressure evolution in the horizontal (a.) and vertical (b.) direction of the cross section. D – drift diameter (adapted from Guayacán-Carrillo et al. [6]).

Fig. 12. Pore pressure evolution induced by tunnel excavation in an isotropic elastic medium with a ratio v/k = 1.5E5 ($t_c/t_p < 1$); v/k = 7.3E5 ($t_c/t_p \approx 1$); v/k = 1.5E7 ($t_c/t_p > 1$). a. Deconfinement rate curves. b. Pore pressure evolution (p/p_0).

Fig. 13. Evolution of confinement ratio λ and of the pore pressure at the tunnel wall. a. Linear pore pressure dissipation very close to tunnel face. b. Pore pressure evolution taking into account the transient coupling effect between fluid flow and deformation.

Fig. 14. Horizontal pore pressure evolution induced by tunnel excavation in isotropic medium with a ratio v/k = 1.5E7, before and after the passage of the face.

Fig. 15. Horizontal pore pressure evolution induced by tunnel excavation in anisotropic medium with a ratio v/k = 1.5E7, before and after the passage of the face. Left side: linear pore pressure rate; right side: non-linear pore pressure rate.

Fig. A.1. Hoop effective stress ($\sigma'_{\theta\theta}$) at tunnel wall obtained from simulation of an excavation with drained boundary conditions. Mesh size variations from 0.03xD to 0.10xD.

Fig. A.2. Pore pressure evolution obtained from simulation of an excavation with drained boundary conditions. Results obtained at tunnel wall and at a distance of $0.2 \times D$ from tunnel wall. Mesh size variations from 0.03xD to 0.10xD.

Fig. B.1. Evolution of pore pressure before passage of the tunnel face. a. Results from Case 1.a. b. Model taking into account undrained elastic parameters. Four points located ahead of tunnel face at a distance of about $0.2 \times D$ are followed. Points are located, in the direction of the *x* axis, at: tunnel axis (A1), tunnel wall (A2), $0.2 \times D$ and $0.5 \times D$ from tunnel wall (A3 and A4).